Substrate-Determined Shape of Free Surface Profiles in Spin-Cast Polymer Blend Films

**A. Budkowski,*,† A. Bernasik,†,‡ P. Cyganik,† J. Raczkowska,† B. Penc,†
B. Bergues,†,⊥ K. Kowalski,†,‡ J. Rysz,† and J. Janik†**

*M. Smoluchowski Institute of Physics and Joint Center for Chemical Analysis and Structural
Research, Jagellonian University, ul. Reymonta 4, 30-059 Kraków, Poland, and Faculty of Physics and
Nuclear Techniques and Faculty of Metallurgy and Materials Science, University of Mining and
Metallurgy, Mickiewicza 39, 30-059 Kraków, Poland*

Received June 10, 2002

ABSTRACT: Sectional views of thin films of symmetric polystyrene/polyisoprene (PS/PI) blends spin-cast from toluene ($C_6H_5CH_3$) onto CH_3- and COOH-terminated self-assembled monolayers (CH_3–SAM and COOH–SAM) show concave- (sharp-edged) and convex-shaped (round) protrusions, respectively, while other morphology features are identical. A 3-dimensional phase domain arrangement was determined with spectroscopic techniques (profiling and mapping mode of dynamic secondary ion mass spectrometry, dSIMS, and X-ray photoelectron spectroscopy). Surface topography was examined with atomic force microscopy and monitored, during the dSIMS analysis, with secondary electrons. In addition, solvent evaporation from PS, PI, and PS/PI layers cast on CH_3–SAM and COOH–SAM was determined. The collected data were used to put forward a model of morphology formation and to elucidate the role of evaporation speed dependent on substrate chemistry in this process, demonstrated here for the first time.

1. Introduction

Thin polymer films are used in a wide range of technological and biomedical applications.[1–6] Blending of polymers can yield materials with desired properties that cannot be provided by a single polymer.[7–8] Free surface topography of polymer blend films, related often with phase domain structure, is critical to the applications.[2–4,9] Both domain structure and topography of the blend films are in the center of increasing interest during the past decade (for a review, see refs 10–16). Initially, the studies were focused on thin blend films confined by flat surfaces and quenched in temperature into two-phase region of the phase diagram.[10–12,17] The role of the competition between the interfacial tension γ and the surface tension difference $\Delta\gamma$ was recognized,[11–13] and a partial-to-complete wetting transition was observed.[18,19] Substrate exchange or $\Delta\gamma$ variation[20,21] leads to different final phase arrangements (such as self-stratified bilayers[10,12,22–23] or laterally separated domains[10,23,24]), while spatial substrate modification results in phase alignment with respect to the patterned substrate (pattern replication[25]). Both types of substrate effects were reflected in (and sometimes coupled with[26]) free surface topography, studied recently in temperature-quenched blend films with deformable air surfaces and different domain structures (stratified,[10,27–29] lateral,[13,27,30–32] or pattern-replicated[26] ones).

While most of the fundamental investigations on blend films have analyzed temperature-driven phase separation, this process is also initiated when a common solvent is added to the mixture. Only recent (and more relevant for the industry) research is focused on the solvent-quenched blend films with deformable free

surfaces,[4,15,16,33–52] formed in the course of rapid solvent evaporation that occurs during spin-casting.[15,16,53,54] Free surface topographies reflect the phase domain arrangement.[33,35,37] Therefore, the role of blend composition[33,34,40–47] or polymer–polymer[15,36–38,43] and polymer–substrate (surface)[35,38,45–46,49–50] interfacial tensions, reported earlier for the phase arrangement in temperature-quenched blend films, was demonstrated also for the surface topography of spin-cast films. Very recently solvent-induced surface undulations of blend[35,55–57] and homopolymer[58,59] films were reported. They are modified when the relevant solvent parameter (polymer solubility[35] or vapor pressure[58,59]) was varied as the solvent was exchanged.

In this paper, we analyze a novel effect, different from those mentioned above. The exchange of the substrate does not affect overall phase arrangement nor lateral features of free surface topography. It has however a strong impact on the shape of free surface profiles, i.e., sectional views of the formed surface undulations. *Concave* (sharp-edged) or *convex* (round) islandlike protrusions are formed for blend films cast on *hydrophobic* or *hydrophilic* substrates, respectively. This substrate effect is examined for symmetric (50/50 w/w) blend films of polystyrene (PS) and polyisoprene (PI), spin-cast from toluene ($C_6H_5CH_3$) onto self-assembled monolayers (SAM) with hydrophobic (CH_3–) or hydrophilic (COOH–) end groups. The present study was stimulated by our earlier results.[45,48,60] The substrate effect was reported in brief in ref 48. General features of surface topography were analyzed with atomic force microscopy (AFM) for various blend compositions (0/100 to 100/0 w/w).[45] Novel extension of dynamic secondary ion mass spectrometry (dSIMS), allowing for a comparison between free surface- and phase-domain-morphology, was introduced in ref 60. Several new results are discussed in this paper in order to gain a better insight into complex processes of morphology formation and to elucidate the substrate effect. First, high-resolution

* Corresponding author. E-mail: ufbudkow@cyf-kr.edu.pl, fax: ++48-12-633 70 86, phone: -632 48 88.
† Jagellonian University.
‡ University of Mining and Metallurgy.
⊥ On leave from Fakultät für Physik, Universität Freiburg, Freiburg, Germany.

AFM images, with relevant but not resolved earlier[45,48] topographic details, are presented. Second, the 3-dimensional phase domain structure is described, as determined with various modes of dSIMS technique and with X-ray photoelectron spectroscopy (XPS). Finally, the critical role of substrate chemistry on solvent evaporation rate is demonstrated based on temporal evolution of the weight of model layers, composed of dissolved pure polymers and their mixtures.

2. Experimental Section

Preparation of Polymer Films. Measurements are reported here for two symmetric (50/50 w/w) PS/PI blend systems and for pure blend components (PS and PI).

The first system is a mixture composed of polystyrene (PS_1, weight-average molecular weight $M_w = 96\ 000$, polydispersity $M_w/M_n = 1.04$) and polyisoprene (PI_1, $M_w = 400\ 000$, $M_w/M_n = 1.12$).[48] The films, used for AFM examination, were cast from toluene onto hydrophobic (denoted as CH_3−SAM with surface tension $\gamma_S \sim 20$ mJ/m^2 [61]) and hydrophilic (COOH−SAM, $\gamma_S \sim 81$ mJ/m^2 [61]) SAM substrates. As SAM substrates, we used Au-covered Si wafers immersed for 60 s in ethanol solutions of 1-hexadecanethiol [$HS(CH_2)_{15}CH_3$] or 16-mercaptohexadecanoic acid [$HS(CH_2)_{15}COOH$].[48,50,61] To produce the Au surface with both SAM (CH_3−SAM and COOH−SAM) regions, half of the wafer was exposed to the solution of $HS(CH_2)_{15}CH_3$ and rinsed with ethanol.[50,61] Then the whole wafer was immersed in the solution of $HS(CH_2)_{15}COOH$.[26,49] Finally, all the substrates were rinsed again with ethanol and dried. Immediately before casting, dry substrates were flushed with fresh toluene and then thin films were prepared by spin-casting (spin speed $\omega \sim 5500$ rpm) from a toluene solution of polymer blend (polymer concentration $c_P \sim 20$ mg/mL) resulting in films with average thickness $d \sim 170$ nm.[45,48]

The second system is the mixture of deuterated polystyrene (dPS_2, $M_w = 174\ 000$, $M_w/M_n = 1.03$) and polyisoprene PI_1 or PI_2 ($M_w = 463\ 000$, $M_w/M_n = 1.05$).[48] Blend films, used for dSIMS and XPS examination, were cast (c_P, ω, and d as above) from toluene onto CH_3−SAM, COOH−SAM or on Si wafers with native oxide layer (SiO_x). In addition, pure homopolymer (dPS_2 and PI_2) films were spin-cast on SiO_x at identical conditions to provide reference samples for XPS. Isotopic PS counterpart, used to provide contrast for dSIMS, and varied molecular weight does not affect the analyzed substrate effect observed for PS_1/PI_1, dPS_2/PI_2, and dPS_2/PI_1 pairs.[48] The SiO_x substrate with intermediate surface tension $\gamma_S = 36.5$ mJ/m^2 [62] (between that of CH_3−SAM and COOH−SAM) was used to trace and discuss details of phase domain arrangement representative for all the substrates used.[45,48] Identical features of the phase domain structure were actually determined for the blend films cast onto SiO_x and CH_3−SAM (see also Supporting Information) as well as on COOH−SAM.

Pure polymers, such as PI_1, PI_2, PS_1, and PS_3 ($M_w = 226\ 000$, $M_w/M_n = 1.06$, used to evaluate the behavior of dPS_2) and their symmetric mixtures (PS_1/PI_2, PS_3/PI_2) were dissolved in toluene ($c_P \sim 20$ mg/mL). A few drops of each solution were cast (conventionally) into a layer on CH_3−SAM or COOH−SAM substrate, positioned immediately on the scale of electronic balance WPS 72 (produced by Radwag) where the solvent was allowed to evaporate over 1000 s at room temperature. Weight of each drying layer was recorded with computer at intervals of 1.1 s.

Characterization of Polymer Films. Free surface topography was examined with CP Park Scientific Instruments AFM microscope working in contact mode[39,49] with the Si_3N_4 cantilevered tip and a typical load of 20 nN.

Horizontal and vertical aspects of phase domain structure in the dPS_2/PI (dPS_2/PI_1, dPS_2/PS_2) films were provided by mapping (lateral resolution of $\sim$120 nm) and depth profiling (depth resolution better than 10 nm) dSIMS modes, respectively.[60] The former yielded lateral composition maps $\Phi_{PS}(x,y)$ of dPS_2 distribution in the film. The latter provided depth profiles of average composition (of dPS_2, PI, all the polymers,
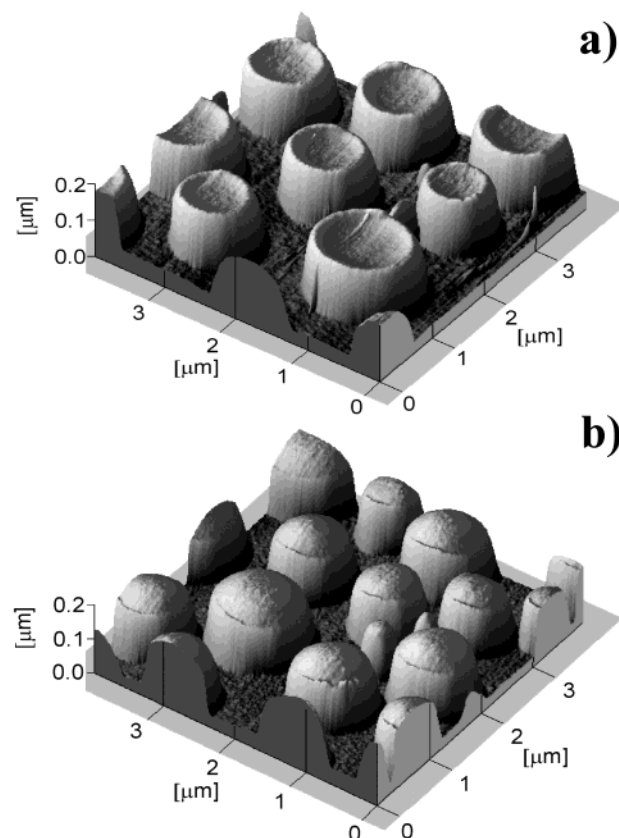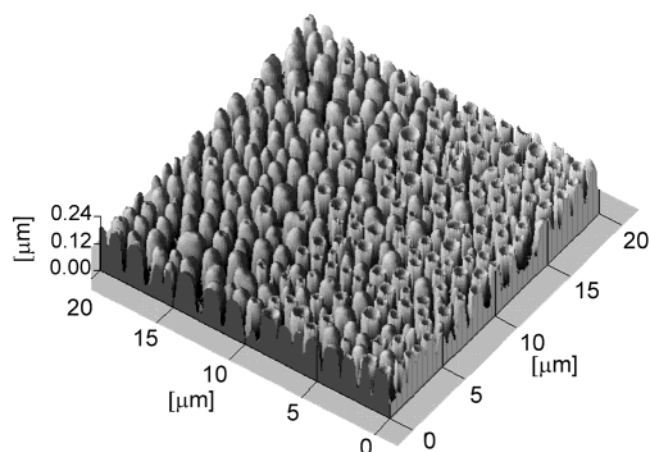
Figure 1. AFM images of free surface topography formed by the PS_1/PI_1 blend films spin-cast onto CH_3−SAM (a) and COOH−SAM (b) substrates.

and Si) recorded for film layers successively exposed with increasing sputtering time (i.e., increasing distance from initial free surface). In addition, topographic maps of these exposed layers were monitored by secondary electron maps.[60] The dSIMS data were obtained with a VSW apparatus equipped with a high-resolution ion gun (double lens, liquid metal, Fei Company) and Balzers quadrupole mass spectrometer using a cylindrical mirror energy filter at the entrance. A primary Ga^+ ion beam (5−25 keV, 0.2−4 nA) was used to sputter the sample and to induce secondary ions and secondary electrons. Secondary ions provided mass-resolved information for the maps and the profiles. The dPS_2 maps (C_2D^-, $m/z = 26$) and the profiles of Si (Si^-, $m/z = 28$) and all the polymers (C^-, $m/z = 12$) were provided by individual signals. To obtain a measure related to fractional concentration of dPS_2 and PI (PI_1 or PI_2) in a polymer film, original signals (CD^-, $m/z = 14$ and CH^-, $m/z = 13$, respectively) were normalized by the $m/z = 12$-yield. The secondary electrons were collected using a Thornley-Evehart-type scintillater/photomultiplier detector. Compositional and topographic images were recorded as 128×128 and 4096×4096 pixel images, respectively.[60]

Surface chemical composition of polymer (dPS_2, PI_2 and dPS_2/PI_2) films was evaluated on the basis of XPS spectra obtained at room temperature using a Specs ESCA spectrometer with Mg Kα source working at 15 kV and 20 mA. The emission angle of photoelectrons was 90°. The sample analysis chamber of XPS instrument was maintained at $\sim$10^{-7} Pa. All C_{1s} peaks were charge referenced to the C−C/C−H peak at binding energy of 285.0 eV.[33,37,63]
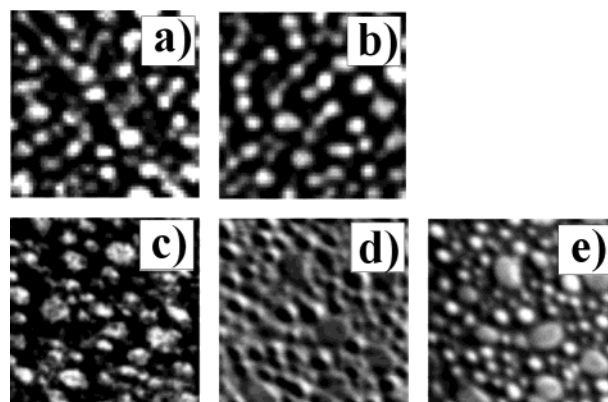
3. Results and Discussion

3.1. Substrate-Determined Shape of Surface Protrusions. Figure 1 shows AFM images recorded for the PS_1/PI_1 blend films spin-cast on CH_3−SAM (Figure 1a) and COOH−SAM (Figure 1b) substrate. Free sur-

Figure 2. AFM image of free surface topography formed by the PS_1/PI_1 blend films spin-cast onto Au substrate covered with COOH−SAM (left upper half of the image) and CH_3−SAM (right lower part).

Figure 3. dPS_2 distribution (a−c) and topography (d, e) maps (28 μm × 28 μm) recorded with secondary ions $m/z = 26$ (a−c) and secondary electrons (d, e) for the dPS_2/PI_1 blend spin-cast on CH_3−SAM (a) and COOH−SAM (b) and for the dPS_2/PI_2 film on SiO_x (c−e). White color marks the regions with high dPS_2 concentration in the film (a−c). Topography maps (d, e; spot different from that in c) reflect the surface exposed after 32 (d) and 115 (e) sputtering cycles and correspond to the data of Figure S2.

face topography exhibits, in both cases, bimodal height distribution. Islandlike protrusions, with circular base perimeter and comparable height and diameter, are visible. The shape of free surface undulations is determined by the substrate chemistry. The sharp-edged (concave) large protrusions are formed for the hydrophobic SAM substrate and the round (convex) ones for the hydrophilic substrate. This effect was also observed earlier for other symmetric PS/PI blends (dPS_2/PI_1, dPS_2/PI_2).[48] For both substrate-types we notice also that steep walls of the circular islands are crowned with a rim. This topographic feature, not resolved earlier for COOH−SAM substrate,[45,48] indicates similarity in morphology formation of both free surface structures (see section 3.4). Elevated regions of the protrusions located inside the rims are concave or convex, enhancing or reducing, respectively, height contrast necessary to reflect these circular rims in the AFM images.

Topographic parameters (e.g., island density) of free surface regions illustrated in Figure 1, parts a and b, are somewhat different, most probably due to, possible, slight modifications of morphology formation conditions in the course of spin-casting. To ensure identical morphology formation conditions we have recorded topography (Figure 2) of the sample with both substrate types, i.e., with CH_3−SAM as well as COOH−SAM region. The left upper half of the AFM image, corresponding to the hydrophilic SAM region, is dominated by convex protrusions. In turn, the right lower part of the image, representative for hydrophobic SAM, is occupied mostly by concave elevations. Height ($\sim$120 nm), diameter ($\sim$1.1 μm) and density ($\sim$0.67 μm^{-2}) of the islands are identical for both halves of the sample. Visible presence of convex large protrusions in the region dominated by the concave ones, and vice versa, is probably related with broad interfacial region between CH_3−SAM and COOH−SAM. Earlier results[48] showed coexistence of concave and convex elevations for the PS/PI blend films cast on substrates with intermediate surface tension, such as SiO_x or Au substrate covered with a mixture of CH_3- and COOH-terminated alkanethiols. The identity of overall topography parameters for free surface undulations formed by the symmetric blend films on CH_3−SAM and COOH−SAM (suggested by Figure 2) was confirmed by rigorous studies applying the integral-geometry approach[45] to an

another (dPS_2/PI_1) system. This conclusion is, in fact, valid for almost all blend compositions.[45] Substrate-determined shape of the elevations was observed for the films with symmetric or nearly symmetric (60/40 w/w) blend composition, where the height of the protrusions is maximal.[45] The substrate effect, detected for protrusions of the films cast from toluene (good solvent for PS and PI), cannot be observed for the blends spin-cast from a solvent with disparity in the solubility of both polymers[48] (e.g., carbon tetrachloride, cyclohexane, or chloroform). In this case the formed free surface topographies do not exhibit a bimodal height distribution and the elevations are not well-defined.

3.2. Domain Structure Determined with Spectroscopic Techniques. Horizontal Domain Structure. Parts a−c of Figure 3 represent lateral composition map of dPS_2 distribution in the films of symmetric dPS_2/PI mixtures spin-cast on CH_3−SAM, COOH−SAM, and SiO_x,[60] respectively. Separated circular dPS_2-rich domains embedded in the PI matrix are visible for all the substrate types. Topological and morphological features of these composition maps correspond to those of topography images recorded with AFM (Figures 1 and 2) and secondary electrons (Figure 3d,e; cf. Figure 3c) for the PS_1/PI_1 and dPS_2/PI_2 blend films, respectively. The latter data are also representative for the free surface, since topographic electron images recorded for different sputtering times (Figure 3, parts d and e) are very similar. We can relate the phase domains rich in PS with the protrusions above the base level of the PI matrix. This confirms the earlier identification based on the AFM analysis combined with a selective dissolution.[48] It is also in accord with linear relation between the fraction of elevated regions and the PS blend composition.[45] The protrusions observed for dPS_2/PI_2 (Figure 3d,e) are more polydisperse than those recorded for PS_1/PI_1 (Figures 1,2), most probably reflecting (for substrate, $M_w - s$ and critical composition changed) a shifted onset of compositional transition to bicontinuous morphology.[45]
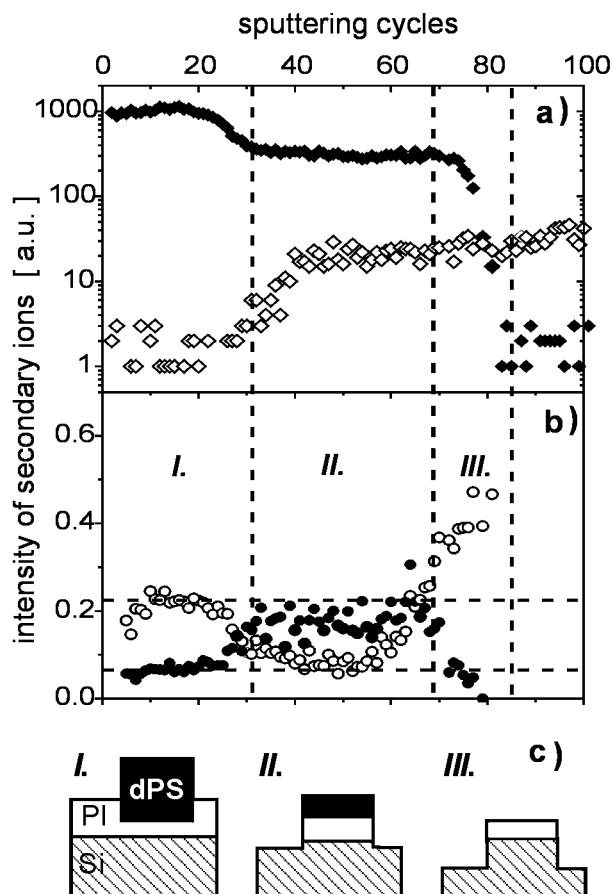
Surface Composition. The profiling dSIMS mode working with a low sputtering rate (ca. 0.5 nm/cycle) was used to trace PI composition in the upper dPS_2/PI_2 film region adjacent to the undulated free surface.[60]
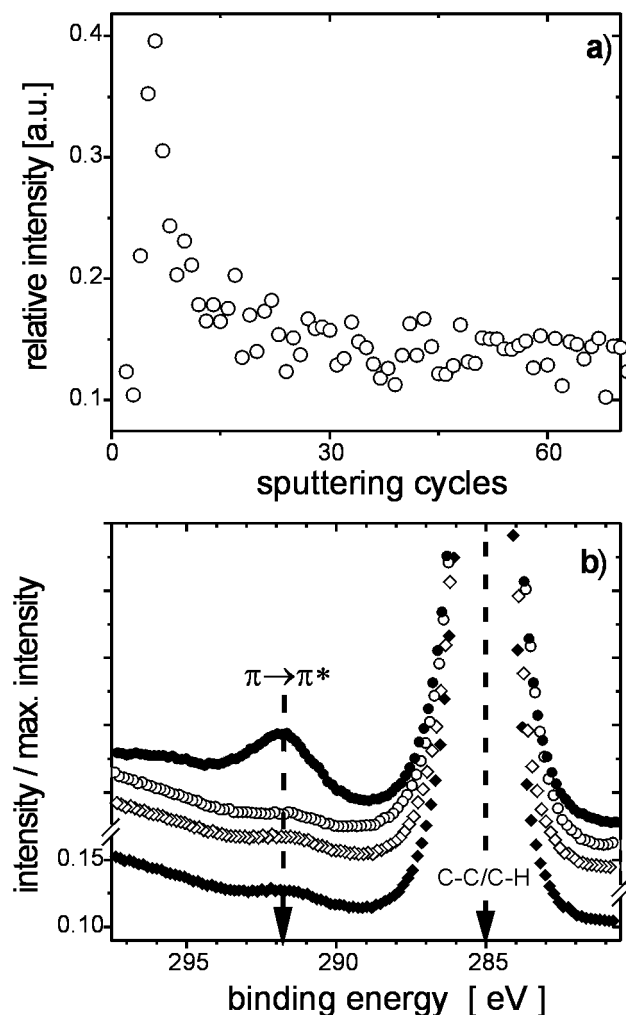
Figure 4. (a) Surface composition of dPS_2/PI_2 blend film spin-cast on SiO_x substrate. Average PI fractional composition (arbitrary units, $m/z = 13$-signal normalized by $m/z = 12$-yield) vs distance from the free surface (one sputtering cycle ~ 0.5 nm). (b) XPS C_{1s} core-level spectra of dPS_2/PI_2 mixture (open diamonds) as well as dPS_2 (solid circles) and PI_2 (open circles) reference films, all positioned on SiO_x. Solid diamonds mark the corresponding spectrum of dPS_2/PI_2 blend spin-cast onto Au covered in halves by CH_3—SAM and COOH—SAM. Positions of the main (C—C/C—H) peak and the maximum of $\pi \rightarrow \pi^*$ satellites are marked by dashed arrows.

Figure 4a shows the average PI_2 concentration, determined for the blend cast on SiO_x, plotted vs the distance from the free surface. A distinct peak, centered at ~3 nm depth, suggests a surface layer enriched in PI_2 with a thickness smaller than the depth resolution, i.e., $d_{PI} \leq 10$ nm. XPS measurements were performed to verify the existence of this thin PI layer covering the free surface. Figure 4b shows the XPS C_{1s} spectra determined for the dPS_2/PI_2 blend films (open diamonds) as well as for the reference homopolymer films of dPS_2 and PI_2 (solid and open circles, respectively), all positioned on SiO_x. An additional spectrum (solid diamonds) measured for the same mixture spin-cast onto Au substrate covered in halves by CH_3—SAM and COOH—SAM is also presented. The dPS_2 spectrum exhibits main C—C/C—H peak centered at the binding energy of 285.0 eV (with unresolved saturated hydrocarbon and aromatic carbon components[63]) and its shake-up satellites corresponding to the $\pi \rightarrow \pi^*$ transition of the benzene ring shifted by ca. 6.8 eV.[63] Only the main C—C/C—H peak

Figure 5. Vertical phase arrangement of the dPS_2/PI_1 film on COOH—SAM as determined with profiling dSIMS mode. (a, b) Profiles corresponding to total polymer composition ($m/z = 12$, solid diamonds), average Si concentration ($m/z = 28$, open diamonds), the fraction of dPS_2 ($m/z = 14$, solid circles) and PI_1 ($m/z = 13$, open circles) in the polymer film (two last signals normalized by $m/z = 12$). Sputtering time measures the distance from original free surface (1 cycle ~ 2.8 nm). Lines are a guide to eye. (c) Sketch to illustrate a sectional view of the sample and phase domains exposed in consecutive sputtering periods. The shape of the protrusions as well as very thin PI surface layer (Figure 4) is neglected for the sake of clarity.

(with unresolved components due to saturated and unsaturated hydrocarbons[63]) is clearly visible in PI_2 spectrum while the $\pi \rightarrow \pi^*$ satellites are much weaker[63] and hardly detected. The spectra corresponding to dPS_2/PI_2 blend films, cast on any of the substrate types used, coincide with the PI_2 spectrum. The absence of distinct $\pi \rightarrow \pi^*$ satellites clearly indicates that free surface of the blend film is covered by the PI_2 layer. Since XPS samples depths of ca. 7 nm,[64] these results yield also a thickness evaluation for the PI layer $d_{PI} > 7$ nm. Comparison with the value determined from dSIMS data leads to the final estimate $d_{PI} \sim 8-10$ nm.

Vertical Domain Structure. To determine vertical phase arrangement in dPS_2/PI blend films the profiling dSIMS mode was used working with high sputtering rate (ca. 1.3−3.5 nm/cycle). Results obtained for the blend films spin-cast onto COOH—SAM (Figure 5) as well as on CH_3—SAM and SiO_x (Figures S1 and S2 of the Supporting Information) are similar. They are exemplified by the data corresponding to the dPS_2/PI_1 blend film on COOH—SAM. Figure 5a represents the determined profiles of secondary ions corresponding to C (solid diamonds) and Si (open diamonds) plotted vs

sputtering time. The profiles, characteristic for polymer film and its substrate, exhibit four consecutive periods (best characterized by different regions of C profile on the logarithmic plot). Three of them can be detected also in the plots of normalized secondary ion intensities corresponding to the fractional concentration of dPS_2 (solid circles) and PI_1 (open circles) in the polymer film (Figure 5b). Topographic maps of the surfaces exposed for various sputtering times, illustrated by Figure 3, parts d and e, were all very similar. This suggests that characteristic sectional view of the surface is not lost due to etching. We propose to relate the four sputtering periods with the following situations (see Figure 5c). First, continuous undulated blend film is present. Second, lower blend regions occupied previously by PI_1 are completely etched (Si is exposed, dPS_2 fraction in the blend layer left is increased). Third, originally elevated dPS_2-rich domains are sputtered away leaving, located beneath and now unprotected, PI_1 remnants (increasing temporarily the PI_1 fraction in the blend film). Finally, all the polymer material is etched. The performed analysis reveals the phase domain arrangement with the dPS_2-rich columns embedded in the PI-rich layer adjacent to the substrate (see Figure 5c, sectional view I). Assuming identical sputtering rate for PI and dPS_2, we can evaluate the surface elevation of typical dPS_2 phase above the PI-rich matrix as equal to 73(5)% of average dPS_2 height. This value, evaluated for the three films examined, corresponds in Figure 5 to the ratio of etching times $(85 − 31)/69$. The dPS_2-rich column extends vertically into the midpoint of the PI substrate layer (the relevant ratio equals $1 − (85 − 69)/31$). The average film thickness of 168(6) nm, evaluated for the data of Figure 5 ($\sim(31 + 85)/2 \times 2.8$ nm), S1 and S2, accords with the value $\sim$170 nm, determined with AFM.[45,48]

3.3. Substrate Dependence of Solvent Evaporation. Free surface topographies of cast blend films, formed during rapid solvent evaporation, reflect the arrangement of phase domains with different solvent parameters (e.g., polymer swelling).[33,35,37] To test whether the substrate chemistry can modify solvent evaporation from individual polymers and their mixtures, we have studied temporal evolution of the weight of model layers composed of polymer blend or its pure components dissolved in toluene. Parts a–c of Figure 6 show the weight of drying PS_1, PI_2, and PS_1/PI_2 layers, respectively, cast onto CH_3–SAM (open diamonds) and COOH–SAM (solid diamonds) substrate. For both pure polymers and their blend we observe a slower evaporation of toluene for the films positioned on the hydrophobic SAM substrate. The same result was obtained for other homopolymers (PS_3, PI_1), another blend (PS_3/PI_2) or varied ambient conditions (a stronger substrate effect on evaporation kinetics is shown in Figure S3). Since toluene has a methyl group, the presence of this solvent close to the CH_3-terminated SAM is energetically more favorable than at the COOH–SAM substrate. This corresponds to slower toluene evaporation. Substrate modification changes interfacial tension, adhesion or friction (determined by short-range interactions), but it has however little influence on long-range dispersion forces at large distances.[66] Therefore, most likely, the observed substrate-induced modification of evaporation kinetics originates not directly from the changed substrate/solvent interactions but rather from the modified boundary conditions of solvent hydrodynamics. Convec-
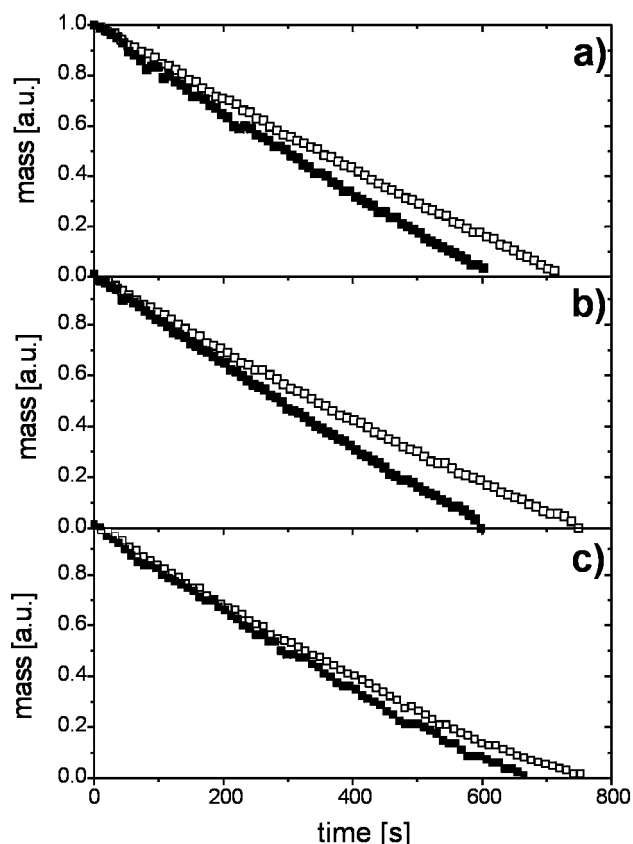

Figure 6. Normalized weight of drying model layers plotted vs evaporation time. The layers composed of PS_1 (a), PI_2 (b), and PS_1/PI_2 (c) dissolved in toluene, were cast onto CH_3–SAM (open diamonds) and COOH–SAM (solid diamonds).

tive instabilities, driven[67] by solvent concentration[67]— or temperature (Bénard-Marangoni)[55]—gradient formed across the film due to solvent evaporation, were reported[55–57,59] or advocated[67] recently for thin[57,59,67] and thick[55,56,67] solvent-cast films of homopolymers and their blends. The role of substrate chemistry was noticed previously in the optimization of experimental conditions necessary to observe convective instabilities.[68] Similarly here, we interpret the evaporation results of Figure 6 in terms of the convection process changed by the substrate chemistry. Convection flows can be involved in the evolution of polymer phase structure domains, emerging in the cast solvent-rich film, and are not restricted to separate polymer domains.[55,56] Therefore, the substrate exchange, modifying solvent hydrodynamics, affects evaporation kinetics in similar manner irrespectively of the polymer domain structure being formed in the drying film (compare Figure 6, parts a, b, and c). Parts a and b of Figure 6 correspond to the evaporation from a single polymer phase (this determines the shape of surface face of fast solidifying domains, see section 3.4). In turn, Figure 6c illustrates total evaporation from different phases in the cast film, possibly affected also by solvent transport from fast- to slow- solidifying phases (see the next section).

3.4 Morphology Formation in Spin-Cast Blend Films. The substrate-determined shape of the free surface profiles was demonstrated for large circular protrusions (Figure 1), constituting the bulk of the elevations. Concave and convex elevated islands were observed for the CH_3–SAM and COOH–SAM substrate, respectively. Smaller protrusions visible sporadically for both substrates (see Figure 7 for CH_3–SAM and Figure
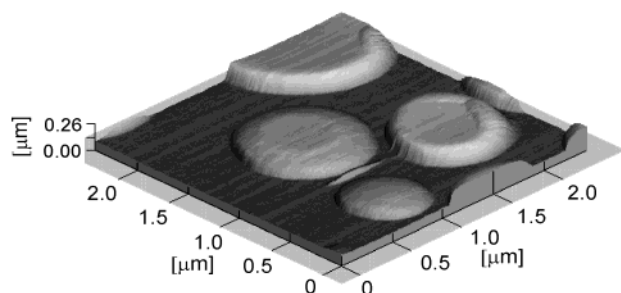
Figure 7. AFM image of the region with large (concave), small (convex) and intermediate protrusions formed by the PS_1/PI_1 blend film spin-cast onto the CH_3−SAM substrate.
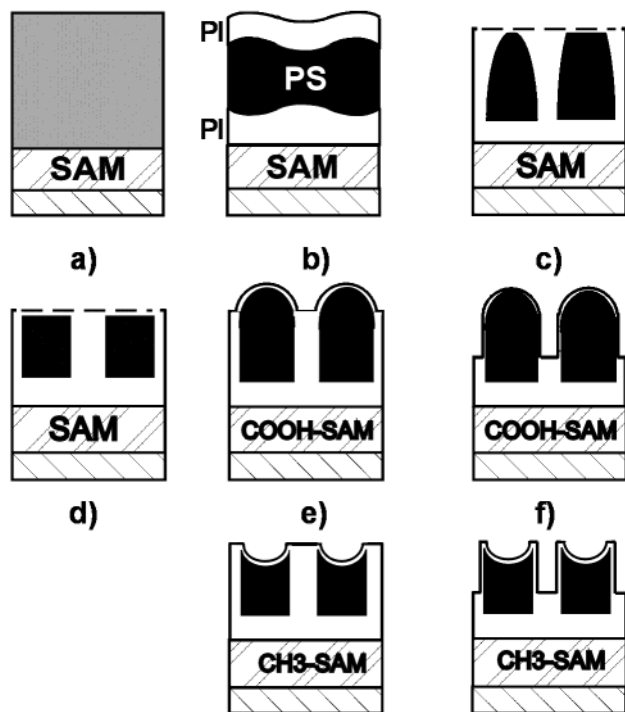
Figure 8. Schematic model describing morphology formation in the PS/PI blend film during spin-casting from toluene on SAM substrate. Subsequent stages of phase domain arrangement correspond to homogeneous (gray) fluid film (a), formation of unstable trilayer PI-rich (white) /PS-rich (black) /PI-rich (b) and its reorganization into lateral phase structure (b–d). Film thickness decreases as a function of time (a–d). Free surface topography is formed (e, f) reflecting lateral domain arrangement. Surface faces of PS-rich domains are frozen as convex- or concave-shaped protrusions for faster (COOH−SAM) and slower (CH₃−SAM) evaporating solvent, respectively. The vertical and horizontal extent of the figures corresponds to hundreds of nanometers and a few micrometers, respectively.

1b for COOH−SAM) are however always round. Figure 7 shows clearly this topographic feature, not resolved previously[45,48] and relevant for the morphology formation model. Small and large protrusions are convex and concave, respectively. In addition, the medium-size islands exhibit intermediate shape of the free surface profile.

The above results allow us to present and discuss now a consistent model (illustrated schematically in Figure 8) accounting for the phase domain structure and the free surface undulations formed in the spin-cast blend films. This morphology formation scenario, presented here to elucidate the substrate-determined shape of the protrusions, is based on extension of earlier models of

homopolymer[53,54] and blend[15,16,34,35,46] films. Although the process is not completely resolved due to mutually coupled multiple effects that cannot be observed directly, its salient and relevant features have been recognized.[15,16,34,35,46,53,54] There are three consecutive stages of the spin-casting. First, most (ca. 90%[53]) of the homogeneous fluid, here composed of PS and PI dissolved in toluene, is spun-off, leaving a uniform film (Figure 8a). Second, the radial flow of the fluid, which is a balance between centrifugal and viscous forces, decreases film thickness and controls its final average value.[53] It is during this stage that phase separation takes place (Figure 8b–d), initiated by decreasing solvent concentration c_S.[15,16,35,46] Third, the arrangement of phase domains is terminated for very low c_S values, when one of the homopolymers is no longer mobile.[46] Lateral domain structure, although frozen in place, is now reflected in free surface undulations (Figure 8e,f) since the rate of solidification due to solvent evaporation as well as polymer swelling in the remaining solvent is different for both polymer-rich phases.[35]

This generally accepted scenario[15,16,35] is extended to include effects specific for the PS/PI system. The preferential attraction of PI to both external surfaces is expected based on earlier observations made for copolymer systems.[18,21,69,70] This is driven by surface tension difference $\Delta\gamma$ (for pure PS and PI at the free surface $\Delta\gamma = 8$ mJ/m² [21]). For polymer blend films with symmetric external surfaces (attracting the same phase), a simultaneous transient wetting of both confining surfaces and phase separation in the film interior is observed.[32] Here, the second stage of spin-casting starts very likely with a formation of unstable[11,12] trilayer PI-rich/ PS-rich/ PI-rich structure in the blend film with a high solvent concentration c_S (Figure 8b). A vestige of this phase arrangement is observed in the fully dried films as a thin PI surface layer and much thicker PI lamella adjacent to the substrate (see the composition profiles in Figures 4a and 5). The trilayer structure breaks up, e.g., due to interfacial[57] or air surface (convective) instabilities (see the next paragraph) (Figure 8b–d), and laterally organized domains are formed as dominant in the final phase structure (Figure 8d–f). This phase rearrangement involves reduction[71] of unfavorable polymer/polymer (PI/PS) interfaces.[11,31,32] The lateral character of the formed PS-rich domains is indicated by Figure 7. The dominant larger elevations (corresponding to PS-rich domains) are constrained to 2-dimensions by the original level of air surface characteristic for solvent-rich film. In contrast, the less abundant smaller domains, which have not reached this level, are always convex. These different domain shapes might possibly reflect various late stages of the coarsening PS-rich domains (Figure 8c,d). The 2-dimensional character of the formed phase domain structures results in the linear relation observed between the PS blend composition and the fraction of the elevated domains.[45]

Convective instabilities can play a role in the phase domain evolution and even determine the final phase structure of polymer blend films.[55–57] It is very likely that the convection is involved also here in the phase rearrangement from the lamellar into the lateral structure. The appearance of separated phase domains can reflect the structure of convection cells.[55] The interdomain spacing (~1.2 μm = $[0.67$ μm$^{-2}]^{-1/2}$ for Figure 2), that is the thickness range expected for solvent-rich film, and partial ordering (e.g., lines in Figure 2) of PS-

rich (elevated) domains suggest here similarity with convection patterns (cf. refs 55 and 56). Convective flows can possibly be involved in substantial thickness reduction of the surface PI-rich lamella and the growth of coarsening PS-rich domains (Figure 7).

The second stage ends with quasi-2-dimensional structure of PS- and PI-rich phases, positioned onto PI-rich lamella wetting the substrate (Figure 8d). In addition, the lateral phase structure is covered with the thin surface layer rich in PI. This phase arrangement is driven by the spreading coefficient ($S = \Delta\gamma - \gamma$) positive for both external surfaces (for pure PS and PI the interaction parameter $\chi = 0.034$;[70] hence, $\gamma \sim 1.4$ mJ/m^2 and $S \sim 6.6$ mJ/m^2 for the free surface). Characteristic encapsulation of the domains of one (PS-rich) phase by the continuous second (PI-rich) phase was observed very recently for another spin-cast blend system.[40,42]

During the third stage of spin-casting (Figure 8e,f), free surface undulations are formed which reflect (frozen in place) lateral domain structure. Two processes are relevant here. First, PS-rich domains solidify with substrate dependent curvature of their surface faces (Figure 8e). Then PI-rich phase collapses below the average height level of the domains rich in PS (Figure 8f). The relevant mechanism was recognized recently.[35] This solvent-related effect, identical for both substrate types (see Figure 2), is a consequence of an earlier solidification of the PS-rich domains as compared with the PI-rich phase (e.g., for pure polymers T_g(PS) = 100 °C and T_g(PI) = −70 °C).[72] The PI-rich regions are swollen with toluene (when domains rich in PS turn solid) and then collapse due to further solvent evaporation. This process is separated in time from that of curvature formation for the PS-rich protrusions. For instance, the circular rims crowning the protrusions (Figure 1, parts a and b) seem to indicate the initial air level of (noncollapsed) PI-rich phase.

The substrate dependent curvature formation of the (PS-rich) protrusions is a novel, so far not reported effect. This process starts when the domains are solvent-rich, most probably already during the second stage of spin-casting. It affects the free surface faces of the lateral PS-rich domains, but does not influence the smaller (always convex) domains, which have not reached the free surface level (Figures 1 and 7). Polymer/polymer interactions[15,36,38] (also in the presence of low m.w. liquid[57,73]) and relative swelling of both polymers[35,72] are not modified by the substrate exchange (CH$_3$−SAM for COOH−SAM). The related change of polymer/substrate interactions does not involve here any variation[35,38,46,49,50] of overall phase arrangement nor lateral features of free surface topography (Figure 2). Therefore, the existing models[15,35,36,38,46,49,50,57] cannot explain[73] the observed substrate dependent shape of the free surface profiles of PS-rich domains.[74] We propose instead to relate it with an another substrate effect, namely with the modification of solvent evaporation (Figure 6). We focus here on the situation close to the point where the substrate-dependent convective flows (see section 3.3) are terminated. Similar to refs 58, 59, and 67, we postulate formation of surface skin depleted of the solvent and a solvent-rich region, which is located deeper in the film. Fast solvent evaporation for COOH−SAM substrate is reflected in positive pressure-difference Δp across the surface skin of PS-rich phase domain. This does not lead to the "bursting" of the solvent, as

reported previously,[59] but rather to the formation of convex domain face in analogy to the process observed for liquid foams.[75] The Laplace pressure Δp,[76] evaluated very roughly for the surface skin, is comparable[77] with the toluene vapor pressure p_{VP}, a value representative for this problem.[67] As the solvent evaporation is fast for COOH−SAM substrate, the formed convex domain faces are frozen before they start to relax toward concave shape reflecting lowered (due to evaporation) pressure of the solvent trapped in the domains. In contrast, the surface faces of PS-rich domains are frozen later for CH$_3$−SAM substrate, i.e., for slowly evaporating solvent and smaller pressure difference Δp. As a result the surface faces are collapsed. More rapid collapse of the surface faces (e.g., due to the solvent "bursting"[59]) leads to a wide size distribution of free surface features (holes),[59] which is not observed here.

4. Summary and Conclusions

Thin films of incompatible polymers spin-cast from a common solvent exhibit free surface topography related with phase domain arrangement. These two aspects of the film morphology are affected when polymer−polymer, polymer−substrate (surface), or polymer−solvent interactions are modified, as reported previously. We demonstrate here, for the first time, the importance of substrate chemistry, which determines the shape of the free surface profiles. The sectional views of the PS/PI blend films cast from toluene on hydrophobic and hydrophilic SAM substrate show sharp-edged (concave) and round (convex) protrusions, respectively, while other features of the film morphology are identical. A detailed film examination with AFM and various spectroscopic techniques (XPS, profiling and mapping mode of dynamic SIMS, and secondary electrons) as well as solvent evaporation measurements allowed us to propose a model (Figure 8) elucidating the morphology formation and the role of convective instabilities modified by substrate chemistry. This modification seems to affect solvent evaporation speed and, as a consequence, also the shape of surface faces of solidified PS domains, but it does not change the overall phase domain arrangement. General features of the free surface profiles (islandlike protrusions) are preserved when the blend film are etched with a keV scale ion beam (Figure 3d,e) indicating that PS/PI blend films can be used as lithographic templates with microscopic and nanoscopic length scale (the latter for reduced $M_w - s^4$). Further experiments are necessary to test whether the curvature of the protrusions could be replicated into the substrate.

Supporting Information Available: Figures showing dSIMS analysis of dPS$_2$/PI blend films cast on CH$_3$−SAM (Figure S1) and SiO$_x$ (Figure S2) substrates and the substrate effect on evaporation kinetics of cast PI$_1$ and PS$_1$ layers (Figure S3). This material is available free of charge via the Internet at http://pubs.acs.org.

References and Notes

(1) Bikson, B.; Nelson, J. K.; Muruganandam, N. *J. Membr. Sci.* **1994**, *94*, 313.

(2) Halls, J. J. M.; Walsh, C. A.; Greenham, N. C.; Marseglia, E. A.; Friend, R. H.; Moratti, S. C.; Holmes, A. B. *Nature (London)* **1995**, *376*, 498.

(3) Berggren, M.; Inganäs, O.; Gustafsson, G.; Rasmusson, J.; Andersson, M. R.; Hjertberg, T.; Wennerström, O. *Nature (London)* **1994**, *372*, 444.

(4) Walheim, S.; Schäffer, E.; Mlynek, J.; Steiner, U. *Science* **1999**, *283*, 520.

(5) Sirringhaus, H.; Kawase, T.; Friend, R. H.; Shimoda, T.; Inbasekaran, M.; Wu, W.; Woo, E. P. *Science* **2000**, *290*, 5499.

(6) Schwarz, A.; Rossier, J. S.; Roulet, E.; Mermod, N.; Roberts, M. A.; Girault, H. H. *Langmuir* **1998**, *14*, 5526.

(7) Bates, F. S. *Science* **1991**, *251*, 898.

(8) Sanchez, I. C. *Annu. Rev. Mater. Sci.* **1983**, *13*, 387.

(9) Arias, A. C.; MacKenzie, J. D.; Stevenson, R.; Halls, J. J. M.; Inbasekaran, M.; Woo, E. P.; Richards, D.; Friend, R. H. *Macromolecules* **2001**, *34*, 6005.

(10) Krausch, G. *Mater. Sci. Eng.* **1995**, *R14*, 1 and references therein.

(11) Binder, K. *Adv. Polym. Sci.* **1999**, *138*, 1 and references therein.

(12) Budkowski, A. *Adv. Polym. Sci.* **1999**, *148*, 1 and references therein.

(13) Geoghegan, M.; Krausch, G. *Prog. Polym. Sci.* **2003**, *28*, 261.

(14) Moons, E. *J. Phys.: Condens. Matter* **2002**, *14*, 12235.

(15) Gutmann, J. S.; Müller-Buschbaum, P.; Stamm, M. *Faraday Discuss., Chem. Soc.* **1999**, *112*, 258.

(16) Budkowski, A.; Bernasik, A.; Cyganik, P.; Rysz, J.; Brenn, R. *e-Polym.* **2002**, *006*, 1 and references therein.

(17) Reich, S.; Cohen, Y. *J. Polym. Sci.* **1981**, *19*, 125.

(18) Rysz, J.; Budkowski, A.; Bernasik, A.; Klein, J.; Kowalski, K.; Jedliński, J.; Fetters, L. J. *Europhys. Lett.* **2000**, *50*, 35.

(19) Geoghegan, M.; Ermer, H.; Juengst, G.; Krausch, G.; Brenn, R. *Phys. Rev. E* **2000**, *62*, 940.

(20) Müller, M.; Binder, K.; Albano, E. V. *Europhys. Lett.* **2000**, *50*, 724.

(21) Rysz, J.; Ermer, H.; Budkowski, A.; Bernasik, A.; Lekki, J.; Juengst, G.; Brenn, R.; Kowalski, K.; Camra, J.; Lekka, M.; Jedliński, J. *Eur. Phys. J. E* **2001**, *5*, 207.

(22) Parry, A. O.; Evans, R. *Physica A* **1992**, *181*, 250.

(23) Bruder, F.; Brenn, R. *Phys. Rev. Lett.* **1992**, *69*, 624.

(24) Flebbe, T.; Duenweg, B.; Binder, K. *J. Phys. II (Fr.)* **1996**, *6*, 667.

(25) Shou, Z.; Chakrabarti, A. *Polymer* **2001**, *42*, 6141 and references therein.

(26) Nisato, G.; Ermi, B. D.; Douglas, J. F.; Karim, A. *Macromolecules* **1999**, *32*, 2356.

(27) Keblinski, P.; Kumar, S. K.; Maritan, A.; Koplik, J.; Banavar, J. R. *Phys. Rev. Lett.* **1996**, *76*, 1106.

(28) Steiner, U.; Klein, J.; Fetters, L. J. *Phys. Rev. Lett.* **1994**, *72*, 1498.

(29) Rysz, J.; Ermer, H.; Budkowski, A.; Lekka, M.; Bernasik, A.; Wróbel, S.; Brenn, R.; Lekki; J.; Jedliński, J. *Vacuum* **1999**, *54*, 303.

(30) Karim, A.; Slawecki, T. M.; Kumar, S. K.; Douglas, J. F.; Satija, S. K.; Han, C. C.; Russell, T. P.; Liu, Y.; Overney, R.; Sokolov, J.; Rafailovich, M. H. *Macromolecules* **1998**, *31*, 857.

(31) Wang, H.; Composto, R. J. *Europhys. Lett.* **2000**, *50*, 622.

(32) Hoppe, H.; Heuberger, M.; Klein, J. *Phys. Rev. Lett.* **2001**, *86*, 4863 and references therein.

(33) Tanaka, K.; Takahara, A.; Kajiyama, T. *Macromolecules* **1996**, *29*, 3232.

(34) Affrossman, S.; Henn, G.; O'Neill, S. A.; Pethrick, R. A.; Stamm, M. *Macromolecules* **1996**, *29*, 5010.

(35) Walheim, S.; Böltau, M.; Mlynek, J.; Krausch, G.; Steiner, U. *Macromolecules* **1997**, *30*, 4995.

(36) Walheim, S.; Ramstein, M.; Steiner, U. *Langmuir* **1999**, *15*, 4828.

(37) Ton-That, C.; Shard, A. G.; Teare, D. O. H.; Bradley, R. H. *Polymer* **2001**, *42*, 1121.

(38) Affrossman, S.; O'Neill, S. A.; Stamm, M. *Macromolecules* **1998**, *31*, 6280.

(39) Cyganik, P.; Budkowski, A.; Raczkowska, J.; Postawa, Z. *Surf. Sci.* **2002**, *507–510*, 700.

(40) Affrossman, S.; Jerome, R.; O'Neill, S. A.; Schmitt, T.; Stamm, M. *Colloid Polym. Sci.* **2000**, *278*, 993.

(41) Müller-Buschbaum, P.; Gutmann, J. S.; Stamm, M. *Macromolecules* **2000**, *33*, 4886.

(42) Chen, C.; Wang, J.; Woodcock, S. E.; Chen, Z. *Langmuir* **2002**, *18*, 1302.

(43) Gutmann, J. S.; Müller-Buschbaum, P.; Schubert, D. W.; Stribeck, N.; Stamm, M. *J. Macromol. Sci.–Phys. B* **1999**, *38*, 563.

(44) Müller-Buschbaum, P.; Gutmann, J. S.; Stamm, M. *J. Macromol. Sci.–Phys. B* **1999**, *38*, 577.

(45) Raczkowska, J.; Rysz, J.; Budkowski, A.; Lekki, J.; Lekka, M.;Bernasik, A.; Kowalski, K.; Czuba, P. *Macromolecules* **2003**, *36*, 2419.

(46) Dalnoki-Veress, K.; Forrest, J. A.; Stevens, J. R.; Dutcher, J. R. *J. Polym. Sci., Part B: Polym. Phys.* **1996**, *34*, 3017.

(47) Dalnoki-Veress, K.; Forrest, J. A.; Stevens, J. R.; Dutcher, J. R. *Physica A* **1997**, *239*, 87.

(48) Bergues, B.; Lekki, J.; Budkowski, A.; Cyganik, P.; Lekka, M.; Bernasik, A.; Rysz, J.; Postawa, Z. *Vacuum* **2001**, *63*, 297.

(49) Cyganik, P.; Bernasik, A.; Budkowski, A.; Bergues, B.; Kowalski, K.; Rysz, J.; Lekki, J.; Lekka, M.; Postawa, Z. *Vacuum* **2001**, *63*, 307.

(50) Böltau, M.; Walheim, S.; Mlynek, J.; Krausch, G.; Steiner, U. *Nature (London)* **1998**, *391*, 877.

(51) Affrossman, S.; Stamm, M. *Colloid Polym. Sci.* **2000**, *278*, 888.

(52) Müller-Buschbaum, P.; Stamm, M. *Colloid Polym. Sci.* **2001**, *279*, 376.

(53) Lawrence, C. J. *Phys. Fluids* **1988**, *31*, 2786.

(54) Schubert, D. W. *Polym. Bull. (Berlin)* **1997**, *38*, 177.

(55) Mitov, Z.; Kumacheva, E. *Phys. Rev. Lett.* **1998**, *81*, 3427.

(56) Kumacheva, E.; Li, L.; Winnik, M. A.; Shinozaki, D. M.; Cheng, P. C. *Langmuir* **1997**, *13*, 2483.

(57) Sprenger, M.; Walheim, S.; Budkowski, A.; Steiner, U. *Interface Sci.* **2003**, *11*, 225.

(58) Müller-Buschbaum, P.; Gutmann, J. S.; Wolkenhauer, M.; Kraus, J.; Stamm, M.; Smilgies, D.; Petry, W. *Macromolecules* **2001**, *34*, 1369.

(59) Strawhecker, K. E.; Kumar, S. K.; Douglas, J. F.; Karim, A. *Macromolecules* **2001**, *34*, 4669.

(60) Bernasik, A.; Rysz, J.; Budkowski, A.; Kowalski, K.; Camra, J.; Jedliński, J. *Macromol. Rapid Commun.* **2001**, *22*, 829.

(61) Genzer, J.; Kramer, E. J. *Phys. Rev. Lett.* **1997**, *78*, 4946.

(62) This value corresponds to the dispersive component of γ_S, see: Zhao, W.; Rafailovich, M. H.; Sokolov, J.; Fetters, L. J.; Plano, R.; Sanyal, M. K.; Sinha, S. K.; Sauer, B. B. *Phys. Rev. Lett.* **1993**, *70*, 1453.

(63) Briggs, D. *Surface analysis of polymers by XPS and static SIMS*, 1st ed.; Cambridge University Press: Cambridge, England, 1998.

(64) Sampling depth of 7 nm for C_{1s} electrons (excited by Mg Kα radiation) in polymeric materials (see Table 2.3 of ref 63) represents all reported values ranging from 5[34,38,40] to 9 nm.[63,65]

(65) Ton-That, C.; Shard, A. G.; Bradley, R. H. *Langmuir* **2000**, *16*, 2281.

(66) Reiter, G.; Sharma, A.; Casoli, A.; David, M.-O.; Khanna, R.; Auroy, P. *Langmuir* **1999**, *15*, 2551.

(67) de Gennes, P. G. *Eur. Phys. J. E* **2001**, *6*, 421.

(68) Kumacheva, E. Personal communication.

(69) Hasegawa, H.; Hashimoto, T. *Polymer* **1992**, *33*, 475.

(70) Budkowski, A.; Klein, J.; Steiner, U.; Fetters, L. J. *Macromolecules* **1993**, *26*, 2470.

(71) Please note that the extent h_e of formed vertical PI/PS interfaces ($h_e \sim 200$ nm) is smaller than that of suppressed horizontal PI/PS interfaces ($h_e \sim 1$ μm), cf. Figure 8d–f and Figure 8b.

(72) Solubility of PI and PS in toluene is similar (as indicated by the solubility parameters δ(PI) = 16.3 MPa$^{1/2}$, δ(toluene) = 17.8 MPa$^{1/2}$, and δ(PS) = 18.7 MPa$^{1/2}$ [48]) and therefore solubility-induced swelling variation[35] is less plausible here.

(73) $S > 0$ is concluded for the following films: (i) prepared at nonzero humidity (PI surface layer is observed), (ii) with water-free polymer blend (see evaluations in the text), and (iii) with any toluene concentration (since $\gamma_{toluene} < \gamma_{PI} < \gamma_{PS}$). Hence PS/PI air contact angle (partial wetting) arrangement is not possible and relevant model[35] cannot be applied.

(74) Test experiment showed that this effect is not influenced by varied humidity (as observed in ref 57).

(75) Weaire, D.; Fortes, M. A. *Adv. Phys.* **1994**, *43*, 685.

(76) Evans, D. F.; Wennerström, H. *The Colloidal Domain: Where Physics, Chemistry, Biology and Technology Meet*, 1st ed.; Wiley-VCH: New York, 1994.

(77) For instance, if we choose $\gamma_{skin} \sim \gamma_{PI}$ and the radius of curvature $R \sim 16$ μm (typical for protrusions of Figure 1b, with 8 μm $< R < 24$ μm), we arrive at $\Delta p \sim 41$ hPa comparable with $p_{VP} \sim 38$ hPa.[58]